

Variable Extended Objects in SA 57

Matthew A. Bershadsky^{1,2}

Department of Astronomy & Astrophysics, Pennsylvania State University, 525 Davey Lab,
University Park, PA 16802

and

Department of Astronomy, University of Wisconsin, 475 N. Charter Street, Madison, WI
53706 (mab@astro.wisc.edu)

Dario Trevese¹

Istituto Astronomico, Universita degli Studi “La Sapienza,” via G.M. Lancisi 29, 00161,
Rome, Italy (trevese@astrom.astro.it)

Richard G. Kron¹

Fermi National Accelerator Laboratory, MS 127, Box 500, Batavia, IL 60510
(rich@oddjob.uchicago.edu)

ABSTRACT

We have isolated a sample of 14 candidate variable objects with extended image structure to $B_J = 22.5$ in 0.284 deg^2 of Selected Area 57. The majority of candidates are blue ($U - B < 0$) and relatively compact. At fainter magnitudes, there is a steep rise in the number of variable objects. These objects are also compact and blue, and some of them are likely to be truly stellar. Twelve of the $B_J \leq 22.5$ candidates have been observed spectroscopically over limited ranges of wavelength and a variety of resulting signal-to-noise. Three of the four brightest have broad emission lines characteristic of Seyfert 1 galaxies. The fourth has a highly variable spectrum consistent with Seyfert-like activity. A fifth candidate has emission line ratios nominally consistent with a Seyfert 2 galaxy. In most cases where we have not been able to confirm a Seyfert spectroscopic type, the spectra are of insufficient quality or coverage to rule out such a classification. Based on spectroscopic and photometric redshift information, the majority of candidates have luminosities less than 10% of

¹Visiting Astronomer, Kitt Peak National Observatory, National Optical Astronomy Observatories, which is operated by the Association of Universities for Research in Astronomy, Inc. (AURA) under cooperative agreement with the National Science Foundation

²NOAO WIYN Queue Investigator

the nominal demarkation between QSOs and AGN ($M_B = -23$, $H_0 = 50 \text{ km s}^{-1} \text{ Mpc}^{-1}$, $q_0 = 0.5$). The surface density of *confirmed* $M_B > -23$ AGN to $B_J = 22$, including stellar sources, is $\sim 40 \text{ deg}^{-2}$, in good agreement with other surveys at this depth. The confirmed AGN in extended sources make up 36% of this population. Thus, the application of a variability criterion to images with extended structure enhances the completeness of the census of active nuclei. If the majority of our candidates are bona fide AGN, the surface density could be as high as 82 deg^{-2} for $M_B > -23$, and 162 deg^{-2} for all luminosities to $B_J = 22$, with extended sources contributing up to 33% of the total.

Subject headings: galaxies: photometry — galaxies: Seyfert — quasars: general

1. Background

We develop techniques for the identification of low-luminosity active galactic nuclei based on their variability. This effort is a direct extension of the survey for variability in images with stellar structure by Trevese *et al.* (1994; T94). Here, we consider images that are detected to be extended, which would be expected to correspond to Seyfert 1 galaxies.

In a series of papers (Kron & Chiu 1981, Koo, Kron, & Cudworth 1986 [KKC], Koo & Kron 1988 [KK88], Trevese *et al.* 1989 [T89], Majewski *et al.* 1991, and Trevese *et al.* 1994 [T94]), we have elaborated a number of search techniques for quasars in Selected Area 57 to faint limits ($B = 22.5$), including colors, lack of proper motion, and variability. These various techniques yield somewhat different samples, which then serve to calibrate the incompleteness of any single technique. However, all of these studies have relied on a parent sample that is restricted to images with structures consistent with star images. One of our results is that the sample of apparently faint quasars is rich in objects that are absolutely faint: according to T94, the sample of 35 quasars has a median luminosity of $M_B = -23.9$ ($H_0 = 50 \text{ km s}^{-1} \text{ Mpc}^{-1}$, $q_0 = 0.5$, $\alpha = -1$), and three quasars have luminosities fainter than $M_B = -22.0$. Five have redshifts smaller than 0.8. Traditionally Seyfert 1 galaxies and quasars are separated at $M_B = -23$ (a distinction we have previously ignored by calling all of the objects in our lists with stellar images and broad lines “quasars”). Clearly there is a likelihood that we have missed some active nuclei in *SA 57* because we have only searched for objects that have stellar image structure. The point of the present investigation is to address this issue, with the goal of extending the completeness of our survey to still fainter absolute magnitudes.

Another result of T94 was that essentially all of the known quasars were detected to be variable, and moreover we argued that the characteristic fractional variability amplitude was generally somewhat higher for active nuclei of lower luminosity. These findings suggest that Seyfert galaxies could be discovered by the property of being variable. Variability is well known to be a common property of Seyfert 1 galaxies, but samples of Seyfert galaxies have been constructed using some other defining criterion, such as spectroscopic characteristics (Cheng *et al.* 1985; Huchra & Burg 1992) or X-ray flux (Maccacaro *et al.* 1991). Hawkins (1983) has consistently advocated the utility of variability as a technique for discovery of quasars. His study, like the present one, was not restricted to images with stellar structure, and he, too, detected some extended images to be variable.

Aside from enhancing the completeness of our catalogue of active nuclei in *SA 57*, there are some more specific motivations to investigate the space density of Seyfert galaxies. The evolution of low-luminosity active nuclei might be very strong at low redshifts, meaning from roughly $z = 0.2$ to $z = 0.4$, as indicated in the luminosity function at $M_B \sim -23.0$

summarized by Hartwick and Schade (1990). At face value, the density of such objects increases from $z = 0.2$ to 0.4 by more than an order of magnitude. However, the sample defining the $z < 0.2$ luminosity function and the sample defining the $z > 0.4$ luminosity function were constructed in different ways, and a wide variety of observational biases can be imagined. A single survey that spanned this range of redshifts would be a valuable check.

For example, since active nuclei can often be detected in the X-ray band, one can investigate the evolution of an optically identified sample defined by X-ray flux. It happens that the Einstein Observatory Extended Medium Sensitivity Survey (EMSS) sample of active nuclei (Della Ceca *et al.* 1994) spans the same redshift range and optical luminosity range addressed here, namely $0.1 < z < 1.0$ and $-21 < M_B < -25$, approximately. For this sample, there is little if any evolution in the X-ray luminosity function, comparing a subsample with $z < 0.3$ with a subsample with $0.3 < z < 0.8$ (Della Ceca *et al.* 1994).

In order to be sure that the result for active nuclei detected in X-rays can be generalized to optically selected active nuclei, we need to know what fraction of the optically selected active nuclei are X-ray sources. Shanks *et al.* (1991) studied a field imaged by ROSAT to a limit in X-ray flux ten times fainter than that of the EMSS, which yielded quasars with a median redshift of 1.5, essentially identical to that of the quasars in T89/T94; even the shape of the distribution at low redshifts is similar. They found that of the known quasars in the field (selected to have $z < 2.2$), 75% of them brighter than $B = 21.2$ were detected by ROSAT. Because of this high fraction, we would not expect that there will be a large number of undiscovered Seyfert 1 galaxies in our field, since otherwise Shanks *et al.* (1991) would have detected an excess of low-redshift sources in their field.

The ability to detect a variable nucleus in a host galaxy depends on a variety of factors, some of which relate to intrinsic properties of the nucleus and host, and some of which relate to observational aspects such the effects of image blur by seeing and the influence of redshift on surface brightness detection thresholds. At a fixed redshift, if the nucleus is too luminous, the source will not qualify as a Seyfert 1 galaxy, and if the nucleus is too faint, it will not be detected to be variable. Even for a fixed ratio of nuclear to host-galaxy light, the detectability of variability will depend on the profile type of the host galaxy: if the light from the host galaxy is relatively extended, it will be easier to isolate the light from the nucleus. Yet another complication is color effects, since the non-thermal nucleus will be bluer than the surrounding star light, and the contrast in a fixed observer’s band will depend on redshift. (Clearly, those nuclei discovered in an optical survey are those that do not suffer large extinction due to dust internal to the host galaxy.)

In this study we devise an operational approach for detecting variability in a sample of extended objects, meaning that there is no special attempt to counteract the selection

effects mentioned above. Rather, we develop an empirical procedure that yields light curves for extended objects based essentially on considerations of the signal-to-noise ratio in a single band (the photographic J , or B_J band, where $B \sim J + 0.1$). In so doing, we can at least put lower limits on the space density of low-luminosity active nuclei at intermediate redshifts in a flux regime not previously explored.

The procedure may find other things, such as galaxies that appear to be variable because of a projected quasar, variable star, or supernova. Projected quasars would tend to have redshifts much higher than plausible for normal host galaxies (and in any case we are interested in finding them). According to T94, variable stars selected in this field at these magnitudes are frequently red; hence a projected star could be recognized by a measured color uncharacteristic of a Seyfert galaxy. The variable stars in *SA 57* also tend to have amplitudes generally lower than the quasars, and when diluted with light from the galaxy image onto which a star was projected, the amplitude would be lower still. In our survey, candidate supernovae would appear only at one epoch, but, as we discuss below, our variability measurement and selection algorithms are biased against finding such events.

2. Procedures

The data and basic procedures are described in detail in T89 and T94. In T89 we considered a catalogue of sources based on plate MPF 1053, which serves as a fiducial epoch against which other plates are referenced. Measurements were obtained on 9 plates over a baseline of 11 years. The plates are homogeneous: all are IIIa-J plates obtained at the prime focus of the Mayall 4-m telescope at Kitt Peak National Observatory. In T89, we established a sample of sources that were 1) nominally stellar and 2) matched with the photometric catalogue of Koo (1986). The latter condition ensures that each source has multi-band (*UJFN*) photometry. After applying a further condition that the sources should have a core magnitude (called m_1) brighter than 24.0 (which yields total magnitudes for stellar sources brighter than about 22.5), the sample analyzed there amounted to 694 sources. In this study, we consider instead a sample that is complementary: it is also matched with the Koo (1986) catalogue, but includes none of the 694 sources studied in T89 and T94.

The photometry consists of aperture magnitudes called m_1 , m_2 , m_3 , and m_4 , according to the size of the aperture. m_1 is the core aperture (central 9 pixels, 0.279 arcsec per pixel), and m_4 corresponds to an aperture with a radius of 1.1 arcsec. The index $m_1 - m_3$ measures the image concentration.

Since the sources have various degrees of angular extent, the magnitude cut is a sliding function of apparent size in order that the limiting signal-to-noise ratio be approximately constant. Specifically, for $m_1 - m_3 < 0.95$, the magnitude cut is $m_2 < 23.5$, and for $m_1 - m_3 > 0.95$, the magnitude cut is $m_2 < 23.5 + 2.5 [(m_1 - m_3) - 0.95]$. For a variety of reasons, our techniques measure bright objects poorly, and we have accordingly further eliminated all objects with $m_4 < 20$. This resulting sample consists of 1636 objects in 1022 square arc minutes.³

The aperture that gives the most robust measure of the magnitude is a function of both image shape and magnitude, for example $m_1 - m_3$ and m_4 . We estimated the values of these so-called optimum apertures empirically by examining the scatter in independent measures of magnitude as a function of aperture size, for samples defined in different bins of magnitude and image concentration. One would expect different plates to have different optimum apertures for the same object, but we found that this extra complication was not warranted: each object is measured with the same aperture on all plates. One difference with respect to the analysis of T89/T94 is that the normalization of the plate-to-plate differences of optimum magnitudes (Δm) is done by fitting a plane to the differences in the space of m_4 and $m_1 - m_3$, instead of fitting line segments to the differences versus m_4 . Table 1 gives specific values for the adopted apertures. After averaging measures at a common epoch and after weighting the plates by their quality, we derive a measure of variability called σ^* for each source. This is essentially the r.m.s. value, after a variety of scale corrections have been applied to ensure that the magnitude system on average matches that of plate MPF 1053 (see T89 and T94 for details).

To provide a statistically consistent variability threshold, we constructed a normalized quantity

$$\sigma_N^* = (\sigma^* - \langle \sigma^* \rangle) / \sigma(\sigma^*),$$

where the mean and standard deviation of σ^* [$\langle \sigma^* \rangle$ and $\sigma(\sigma^*)$, respectively] are measured as a function of m_4 and $m_1 - m_3$. The bivariate distribution of σ^* in m_4 and $m_1 - m_3$ varies little as a function of $m_1 - m_3$ at a given m_4 except at the threshold between stellar and

³In practice, our analysis is conducted on a sample of 2540 sources which satisfy our magnitude cuts. This includes the 1636 sources considered here, the 694 sources studied in T89 and T94, and 210 sources that are not matched with the catalogue of Koo (1986). Source detection for Koo’s catalogue used multiple plates but did not include MPF 1053. Of the unmatched sources, roughly half (107) were found to be on the border of regions excluded from the catalogues of Koo (1986); the remaining unmatched sources were found to have uncharacteristically small $m_1 - m_3$ or large variability. Visual inspection of the brightest of these sources on plate prints revealed they were plate flaws. ‘Unmatched’ sources were excluded from the final list of variable candidates.

non-stellar objects ($m_1 - m_3 = 1.05$). Hence, we simply divided the sample into two bins of $m_1 - m_3$ (< 1.05 and ≥ 1.05), and found $\langle \sigma^* \rangle$ and $\sigma(\sigma^*)$ independently for these two samples. To find the mean σ^* , $\langle \sigma^* \rangle$, as a function of m_4 , we fit a low-order spline function and rejected individual points from the fit if they were more than 3 standard deviations above or below the best fit. This rejection process was iterated three times. The standard deviation about this fit, $\sigma(\sigma^*)$, was then redetermined more precisely using a sliding window in m_4 about each object, adjusted to be wide enough to include a minimum of 100 objects, up to a maximum width of 0.5 mag. Again, objects above 3 standard deviations from the original fitting process were excluded from the calculation. To ensure that the standard deviation changed smoothly with m_4 , we fit a low-order spline to the individual standard deviation measurements as a function of m_4 . Table 2 summarizes the values of the mean and standard deviation of σ^* as a function of m_4 and $m_1 - m_3$ that we used in this analysis to construct σ^*_N .

We note that while the present sample of sources is supposed to have extended image structure, it most likely contains some bona fide stars, especially at the faint end. For example, an object with $m_1 - m_3 < 1.05$ but with $m_1 > 24.0$ would not be included in the source list of T89, but it will appear in the complementary list considered here. A few such objects will have measured $m_4 < 22.5$, bright enough to be reliably measured for variability.

The criterion for variability that we adopt is simple: for $m_4 < 22.5$, the normalized σ^* , σ^*_N , must be larger than 2.5. For comparison, we consider also a secondary sample consisting of 35 sources with $m_4 > 22.5$ and σ^*_N larger than 3.5. The 14 sources in the first list can be considered to be prime candidates, and are listed in Table 3. Two sources in the second list are also included in Table 3 in order to define a sample complete to $J < 22$, as defined by the total magnitudes from Koo (1986). These are discussed in Section 4. All of the sources in Table 3 have extended light profiles as defined both by the criterion $m_1 - m_3 > 1.05$ and by the r_{-2} parameter of Kron (1980). We inspected the images of each of these visually to check for any peculiarities (such as close neighbors) that potentially might influence the photometry. No clear problems were found, but some close neighbors are indicated in the notes to Table 3.

Some cases of candidate variables were matched with more than one object in the Koo (1986) list. Upon inspection, in all cases the present catalogue misses a close object, and it is impossible to recover which particular object was actually measured. It seems very likely that the proximity of two or more objects has resulted in photometric errors that appear as large σ^* . We have deleted from further consideration all cases where there were multiple matches. All of the close neighbors indicated in Table 3 were substantially fainter than the ones resulting in multiple matches.

3. Findings

Figure 1 shows a plot of σ^* versus m_4 for the sample of 1636 objects. The format of this plot is directly analogous to that of Figure 1 of T89. Note that the noise level defined by the majority of non-variable objects is respectably low, and in fact compares well with that for stellar images (i.e. Figure 1 of T89), despite the expected greater difficulty of measuring images with a variety of profile types. The upper envelope of σ^* is quite well-defined for the non-variable objects down to about $m_4 = 22.5$.

The candidate variable objects selected according to the criteria mentioned in the previous section are marked. (Note that at faint magnitudes there is an overlap between the marked and unmarked objects. This occurs because the compact images are normalized differently from the extended images.) The distribution of σ^* for the candidate variables is similar to that of the quasars discussed in T89. In the latter case we had substantial spectroscopic confirmation that the variables really are quasars (and therefore are likely to be truly variable!). In the present case, the spectroscopic confirmation is not as complete.

3.1. Spectroscopic confirmation

Spectra for 12 of the 16 candidates in Table 3 have have been collected over the past decade using KPNO multi-fiber spectrographs on the Mayall 4m telescope (Figure 2a) and more recently on the WIYN 3.5m telescope (Figure 2b).⁴ These spectra were obtained as part of larger redshift survey programs (KK88, Kron *et al.* 1991, Munn *et al.* 1997, Bershadsky *et al.* 1997).

Three candidates in Figure 2a clearly show evidence for the presence of AGN: MgII is detected in Nser 100681 and 114264, and broad H α emission is seen in Nser 110195. For Nser 100681, the MgII line (as well as H β and [O III] λ 4959, 5007) have been independently confirmed from a spectrum taken with the KPNO 2.1m and GoldCam spectrograph (Bershadsky, Trevese, and Kron 1991). For Nser 114264, the MgII identification is less secure because it is so near the blue limit of the spectral range, although it does avoid the telluric absorption feature at 3700 Å and it is at the correct wavelength for the redshift determined from other lines. Notice also the unusual combination of a strong break at 4000 Å *and* the presence of [O III] λ 4959, 5007 emission (H β suffers from being on a sky line). The last object in Figure 2a, Nser 110459, has a secure redshift but no detected line emission; there

⁴The WIYN Observatory is a joint facility of the University of Wisconsin-Madison, Indiana University, Yale University, and the National Optical Astronomy Observatories.

is insufficient evidence for the presence (or absence) of AGN. In the last two cases, increased signal-to-noise and extension of spectral coverage to the blue or red (to cover either MgII or H α) would further secure identification of nuclear activity. The spectrum for one additional object (NSER 116720) is not shown because it has inadequate signal-to-noise to be of value.

Of the more recent spectroscopy shown in Figure 2b, only one candidate’s spectrum (Nser 105334) presents compelling evidence for nuclear activity based on line ratios of [O II] λ 3727, H β and [O III] λ 5007. We estimate $\log([O III] \lambda 5007/H\beta) \sim 0.76 \pm 0.04$ and $\log([O II] \lambda 3727/H\beta) \sim 0.41 \pm 0.02$, where the uncertainties include random errors only. For example, we have made no correction for H β absorption. Also, the spectrum is uncalibrated. To estimate the [O II] λ 3727/H β ratio, we have used nominal throughput values as a function of wavelength, calculated specifically for the adopted instrumental configuration. The estimated values are just on the border of the Seyfert 2 region defined by Tresse *et al.* (1996 and references therein), in a region where some confirmed Seyfert 2’s are found.

One other object in Figure 2b has a secure spectroscopic redshift: Nser 108853. While line emission is evident ([O II] λ 3727 and possibly [O III] λ 5007), the spectrum does not cover H α or MgII. The other four objects in Figure 2b also show line emission, however either there is only one line (identified as [O II] λ 3727 for Nser 113571, [O III] λ 5007 for Nser 107772 and H α for Nser 118640), or the line is near a strong sky line (Nser 106596). For the two cases where either MgII or H α is supposed to be within the spectral range, the redshifts are uncertain.

Lastly, there is one object (Nser 104326) for which we have obtained two spectra, \sim 6 years apart (Figure 2d). Both spectra were observed with identical apertures (3 arcsec diameter fibers). While the first spectrum shows only one probable emission line ([O II] λ 3727) the second spectrum shows strong (and narrow) [O II] λ 3727, and [O III] λ 4959, 5007 at $z = 0.215$. The first spectrum also has a very blue (rising) continuum below 5500 Å. While the second spectrum is not flux calibrated, it shows a strong (Balmer) break not present in the first, and a redder continuum below 5500 Å; these differences are not attributable to the lack of calibration in the more recent spectrum. This object exhibits spectral variability which we identify as Seyfert-like activity.

In summary, three objects are definitely confirmed Seyfert 1’s (Nser 100681, 110195, 104326), one object is likely a Seyfert 1 (Nser 114264), and a fifth (Nser 105334) has line ratios marginally consistent with a Seyfert 2. We identify these five as ‘confirmed’ AGN. Of the remaining six spectroscopically observed candidates, none can be definitively ruled out as AGN on the basis of the available spectra.

3.2. Candidates at $m_4 < 22.5$

There are many possible reasons why an extended image might erroneously be selected as a variable, and without additional arguments, one does not know how seriously to take the remaining unconfirmed candidates. First, we can ask whether the number of candidates in Table 3 is reasonable given expectations for the number of Seyfert 1 galaxies to this depth. Such an estimate was made by R. Burg (1987), who predicted the counts of Seyfert 1 galaxies based on the statistics of active nuclei seen in the CfA survey. According to this estimate, 24 Seyfert 1 galaxies are expected in this area to this depth. But, our survey is sensitive only to a particular subset as outlined in Section I, and on this basis the actual number of candidates seems to be broadly reasonable. Moreover, as mentioned earlier, the results ROSAT identifications by Shanks *et al.* (1991) constrain the population of active nuclei at $B \sim 21$, with similar conclusions.

One possible source of ‘contamination’ in our sample may be supernovae. A supernova explosion within a galaxy could sufficiently alter the galaxy’s luminosity to give it a variability index that would fall above our selection threshold. In this case, however, one would expect the light curve to change (brighten) only at one epoch. The light curves of the candidate variables, shown in Figure 3, indicate that only two objects plausibly fit this pattern (Nser 104326 and 114264). Inspection of the images of these sources at the appropriate epochs show no supernova events. Moreover, for both of these objects there is spectroscopic evidence for Seyfert-like activity. In short, there is no compelling evidence that supernovae are significant contributors to the variability of our candidates. Indeed, we would not expect to find supernovae in our sample of variables because the anticipated total number of supernovae events is small,⁵ and our variability algorithm is not optimized for supernovae: the apertures used to measure variability enclose a small fraction of the total apparent galaxy area in a central region where the light profile is brightest (worst contrast), and our glitch-suppression algorithm (see T89) favors throwing out single epochs of large variability. The absence of supernovae events in our sample therefore should *not* be used to constrain supernovae rates in faint galaxy samples. Our variability algorithm is well suited for finding on-going nuclear variability of low to moderate amplitudes.

If the list of candidate variables indeed consists of mainly Seyfert 1 galaxies, we would

⁵Scaling from the results of Pain *et al.* 1996, who find 34_{-16}^{+24} supernovae $\text{yr}^{-1} \text{deg}^{-2}$ for $21.3 < R < 22.3$, we estimate there should be 0 to 3 supernovae in our entire series of plate images. The scaling accounts for smaller area (0.284 deg^2), shallower depth (translating to roughly a factor of two lower galaxy surface density), and a sampling of the equivalent of 0.3 yr (7 epochs, each spaced by > 1 year, and estimating supernovae will be bright enough to raise our variability index above threshold for 15 days).

expect the distribution of $m_1 - m_3$ indices to show a tendency to small (compact) values, since the nucleus should affect the overall profile. Figure 4 plots $m_1 - m_3$ versus m_4 to explore this possibility. The five objects confirmed spectroscopically to have active nuclei indeed have smaller $m_1 - m_3$ than the parent sample, with the exception perhaps of Nser 104326. In general, the candidates at $m_4 < 21.7$ appear to be generally compact, whereas the fainter candidates ($21.7 < m_4 < 22.5$) are not clearly distinct from the parent sample in this index. This could suggest either that the lists of candidates becomes less reliable with increasing faintness, or that the errors in $m_1 - m_3$ grow with increasing m_4 (but the reliability remains high), or that the fainter Seyferts are, in fact, more extended. Without further information, it is difficult to distinguish between these possibilities.

As previously mentioned, active nuclei are expected to be bluer than the host stellar population, especially in a color index like $U - B$. We therefore check the color distribution. We have taken the $U - J$ color index from the Koo (1986) catalogue, and plot it in Figure 5 versus m_4 . The distribution of the candidate variables in this plot with respect to the parent population follows very much the same trends as noted for Figure 4, namely: The five objects confirmed spectroscopically to have active nuclei (including Nser 104326) clearly fulfill the expectation of bluer $U - J$ colors. The candidates at $m_4 < 21.7$ are somewhat bluer than the rest of the population, and the fainter one ($21.7 < m_4 < 22.5$) are typical of the population.

The bivariate distribution in $U - J$ color and $m_1 - m_3$ image compactness indices, illustrated in Figure 6(a), also reveals the $m_4 < 22.5$ candidates are distinct from the rest of the population. Here, however, even the $21.7 < m_4 < 22.5$ candidates are distinct. It appears that the color distribution for the candidate variables is more clearly distinct from the parent population than the size distribution. Note in particular the absence on any candidates in the clump of points centered at roughly $U - J \sim 0.8$ and $m_1 - m_3 \sim 1.15$. This clump corresponds to normal galaxies with red colors and large bulges such as types E and Sa.

A priori, it is not obvious how, or if the light curves of the variable candidates will show correlations with other observables. The light curves for the five reddest candidates ($U - J > 0$) all show large amplitude (0.5 mag) changes between epochs. Four of these are the faintest at the same epoch. Inspection of the spatial locations of these objects, however, shows they are randomly positioned in the field. Therefore this coincidence is not likely the result of a plate flaw. One of the bluest objects also is faintest at this epoch and has a comparably large amplitude change. Hence there is no strong indication that the light curve amplitude and shape correlate with color. The shapes of the light curves also show no obvious trends with either m_4 or $m_1 - m_3$.

Finally, we can use the spectroscopic redshift information to explore whether the candidates are unusually distributed in luminosity or redshift. The Hubble diagram in Figure 7 compares the 14 variables candidates with spectroscopically confirmed galaxies (Munn *et al.* 1997) and QSOs (Kron *et al.* 1991) in the same field. For candidates without spectroscopic redshifts, photometric redshifts are calculated using a method similar to that described by Connolly *et al.* (1995).

The five objects confirmed spectroscopically to have active nuclei span a large range in luminosity. The apparently brightest candidates, Nser 100681, is also the most luminous extended source in the field, while Nser 105334 is roughly at $0.1 L^*$.⁶ One other source (Nser 106596) is exceptionally luminous, but its spectroscopic redshift is uncertain. Were it placed at its photometric redshift, its luminosity would be $\sim L^*$. Nonetheless, while the bulk of the candidates appear typical in luminosity of the rest of the field galaxy population, *the redshift distribution is skewed to higher values.* With the exception of Nser 118640, the variable candidates are all at or *above* the median redshift of the field galaxy sample ($z \sim 0.22$ for $B_J = 22.5$). Nser 118640 is itself in an unusual region of the Hubble diagram.

The photometric redshifts in the above analysis are in principle prone to systematics if the sources are dominated by AGN light. Systematics might arise because the “training set” used to calibrate the photometric redshift relationship contains excludes AGN. In other words, the mapping of redshift onto the space of $UJFN$ apparent magnitudes is done for different types of spectral energy distributions. Indeed, of the five confirmed AGN, the dispersion between the spectroscopic and photometric redshift is 0.18 in redshift, roughly 3.5 times larger than the average galaxy to $B_J < 22$ using the same photometric data. On the other hand, the difference between spectroscopic and photometric redshifts for the same five objects is close to zero in the mean. At the very least, photometric redshifts are useful here for identifying if the candidates have unusual colors. It appears likely, however, that photometric redshifts are reliable for these candidates on average, but unreliable for individual targets.

Overall we conclude that Table 3 does contain many bona fide active nuclei. This impression is based on the success of spectroscopically identifying five objects; the bivariate distribution in color and image structure; the distribution in redshift; and the sharp upper envelope of points in Figure 1. At minimum, Table 3 can be considered to be a good list for further spectroscopic investigation.

⁶We use L^* to refer to the normal galaxy luminosity function and corresponds to $M_B \sim -21$ for $H_0 = 50$ km s⁻¹ Mpc⁻¹

3.3. Candidates at $m_4 > 22.5$

The fainter candidates, $m_4 > 22.5$, likely comprise a number of truly stellar objects that were missed in our previous survey because of the way we applied selection cuts to the parent sample. Indeed, over half (19 out of 35) of these variable candidates have $m_1 - m_3 < 1.05$, and hence are consistent with stellar image profiles. Of the 19 $m_4 > 22.5$ candidates with $m_1 - m_3 < 1.05$, however, about half (nine) are classified by Kron (1980) as extended.⁷ Yet of the 16 $m_4 > 22.5$ candidates with $m_1 - m_3 > 1.05$, only two of these are classified by Kron (1980) as stellar. Hence there is some indication of extended image structure for over 90% of this faint sample.

At the bright end of the $m_4 > 22.5$ candidate list, one object (Nser 17671) is independently selected as a QSO candidate from KKC (#6, $m_4 = 22.54$). This is an object classified as stellar by Kron (1980), but extended based on a value of $m_1 - m_3 = 1.134$. Nser 17671 has a tentative spectroscopic identification as a narrow emission-line galaxy at $z = 0.518$ based on a single line identified as [O II] $\lambda 3727$ (KK88, Table 1, #73). The spectrum, however, does not go blue enough to detect Mg II, or red enough to detect H α . Majewski *et al.* (1992) also find this object to be variable and with no detectable proper motion.

At the faint limit of the $m_4 > 22.5$ candidate list, three other objects are found in Majewski *et al.*'s sample. Two have $B_J > 23$. All three are stellar according to the $m_1 - m_3$ criterion and Kron (1980). None pass Majewski *et al.*'s variability threshold, while two have detectable proper motions (one of which is very large). However, all three objects have $U - J > 1.75$ (one is not shown in Figure 6b because it is a U band dropout). Indeed, these are the only three objects in the faint sample with such red colors, and they are likely to be stars (*cf* Figure 3 of T94).

Figure 6(b) shows the $m_4 > 22.5$ candidates in a plot similar to Figure 6(a), which reveals a disproportionate number of candidates with blue $U - J$ colors and compact image structure. This is expected if the fainter sample has a higher fraction of blue stellar sources which are bona fide quasars. The remaining variable candidates, with $m_1 - m_3 > 1.05$, are typically equally as blue as the stellar candidates. Without spectroscopic confirmation the reliability of this fainter sample is unknown. In general, however, the variability amplitudes of the fainter candidates (Figure 1) are consistent with those of known quasars.

⁷Kron classified image profiles on the basis of their second inverse moment, r_{-2} . In general r_{-2} and $m_1 - m_3$ are highly correlated. Different classifications based on these two indices reflect different sensitivities to a variety of image profiles, as well as noise. A comparison of r_{-2} to $m_1 - m_3$ for comparably faint objects in this field can be found in Koo *et al.* (1986).

4. The surface density of AGN to $B_J = 22$

We define B_J operationally here as J_K , listed in Table 3, because this magnitude is a good approximation to a total magnitude, independent of image size and shape. A sample of extended variable objects, complete to $B_J = 22$, can be constructed by (i) adding two fainter candidates (Nser 101951 and 107772) to our primary sample defined by $m_4 < 22.5$; but (ii) removing the faintest $m_4 < 22.5$ candidate with $B_J > 22$ (Nser 105334, a confirmed AGN). This ‘complete’ sample is useful for assessing the surface density of AGN: at these depths the spectroscopic completeness of our QSO survey in *SA 57* is relatively high (Kron *et al.* 1991), and other surveys exist for comparison (e.g. Zitelli *et al.* 1992).

The two additional extended variable candidates are only ~ 0.25 mag fainter than our primary sample limit in m_4 , and all indications are that these two objects are good candidates. For example, both are blue ($U - J < 0$). Their light curves (Figure 3) are also comparable to the brighter candidates with the one exception that the 7th epoch is excluded from the estimate of σ^* for Nser 107772. (This exclusion is mandated by a glitch-suppression algorithm, described in T89.) Based on m_1 - m_3 , Nser 107772 is quite compact, with $U - J$ comparable to the confirmed AGN. Yet while it would be considered ‘stellar’ on the basis of m_1 - m_3 , it has a large r_1 and is classified as a galaxy in the catalogue of Koo (1986). In short, Nser 107772 appears to be large, blue galaxy with a compact core. Both objects are among the apparently largest galaxies for their apparent magnitude.

In total, there are 15 extended variable candidates to $B_J = 22$, four of which are spectroscopically confirmed AGN. In comparison, there are 26 confirmed QSOs (i.e. AGN with stellar image structure) in *SA 57* to the same limit. In addition, there are five *stellar* objects satisfying high variability and lack of proper motion but without spectroscopic confirmation (T94). Because all other *stellar* objects meeting these variability and proper motion criteria are bona fide QSOs, we assume here that these 5 objects are also QSOs. Adding our four confirmed extended variables to the 31 QSOs yields a total surface density of $123 \pm 21 \text{ deg}^{-2}$ in *SA 57*.

Zitelli *et al.* (1992) find a similar surface density, $115 \pm 16 \text{ deg}^{-2}$, to the same magnitude limit, and in a separate field. Their sample is 100% spectroscopically confirmed. Yet in the limiting case where all of our extended variables are bona fide AGN, the surface density in *SA 57* would reach $162 \pm 24 \text{ deg}^{-2}$, with extended sources contributing 33%. Zitelli *et al.* use color and variability selection strategies for stellar sources similar to our own. There are, however, a few differences between the surveys. For example, we have proper motion information, whereas their sample includes selection by spectroscopic features seen on a grism plate. One other difference is that they do not specifically target sources with extended image structure.

Based on spectroscopic and photometric redshift information, the majority of our extended variable candidates have luminosities less than 10% of the nominal demarkation between QSOs and AGN ($M_B = -23$, $H_0 = 50 \text{ km s}^{-1} \text{ Mpc}^{-1}$, $q_0 = 0.5$). This luminosity estimate is an upper limit since the measured apparent magnitude is within a large aperture that includes a non-negligible contribution of light from the host galaxy. The surface density of *confirmed* $M_B > -23$ AGN to $B_J = 22$, including 7 stellar sources and four extended sources, is $39 \pm 12 \text{ deg}^{-2}$, again in good agreement with Zitelli *et al.*'s value of 40 ± 9 . In the limiting case where all of our extended variable candidates are bona fide AGN, and we include $5 \times \frac{7}{26}$ of the unconfirmed, non-moving stellar variables (5 is the total number of unconfirmed, non-moving stellar variables; $\frac{7}{26}$ is the fraction of confirmed QSOs with $M_B > -23$), the surface density would reach $82 \pm 17 \text{ deg}^{-2}$ for $M_B > -23$ with extended sources contributing 64%. The majority of the unconfirmed AGN are between $0.2 < z < 0.4$, whereas Zitelli *et al.* find no AGN at $z < 0.4$.

The total number of extended variable candidates corresponds to $\sim 2\%$ of the surface-density of all extended sources to $B_J < 22$. These candidates vary at roughly > 0.1 mag. In contrast, Kochanski *et al.* (1996) find only 0.74% of all sources vary by 0.026 mag or more to the same magnitude limit. However, T89 found $\sim 9\%$ of the stellar sources vary at roughly > 0.1 mag to $B_J < 22.5$ (or $\sim 5\%$ to $B_J < 22$). T89's result is roughly two orders of magnitude higher than Kochanski *et al.* (by Kochanski *et al.*'s estimate) for stellar sources. Yet T89's sample of candidate stellar variables independently identified spectroscopically confirmed QSOs with high completeness and reliability. Similarly, we have spectroscopically confirmed that at least one third of our extended variable candidates are bona fide AGN. Further, as we have discussed in Section 3.2, the number of extended variable candidates is comparable to the total number of Seyfert 1's expected at this magnitude limit. We conclude, therefore, that the surface density of variable sources we find is likely reliable.

5. Summary

We have shown that it is possible to select AGN in sources with extended light profiles on the basis of variability alone, in a manner similar to that which we have successfully identified stellar AGN (QSOs). A posteriori, several of our extended variable candidates have been confirmed spectroscopically to be bona fide AGN. However, we still lack adequate spectroscopy to confirm or rule out the existence of nuclear activity for the majority of our sample. The color and size distributions of the candidates shows that at brighter magnitudes the sample is preferentially bluer and more compact than non-variable galaxies.

The confirmed AGN are in this magnitude range. At fainter magnitudes, the sample is more representative of the entire population of extended sources. The redshift distribution of the sample, however, is skewed to values above the median for normal galaxies at the depth of this survey. On these bases, and from our preliminary spectroscopic success, we believe we have identified a sample worthy of further spectroscopic investigation. If all of these candidates are bona fide AGN, this represents a 30% increase in the surface density of all AGN (i.e. including QSOs) at $B_J = 22$. At the very least, AGN which appear extended in ground-based images with ~ 1 -1.5 arcsec seeing represent 10% of the total AGN population.

We gratefully acknowledge Dave Andersen for assistance with reducing WIYN/Hydra spectra and estimating photometric redshifts; Alessandro Bunone for photometric error estimates; Steve Majewski for information from his proper-motion survey; and Jeff Munn and David Koo for their efforts in producing the spectra from the Kitt Peak Galaxy Redshift Survey. We thank Di Harmer and other members of the NOAO WIYN Queue team for assistance in gathering spectroscopic data. MAB acknowledges support from the Italian CNR; NASA through Graduate Fellowship NGT-50677 and Hubble Fellowship HF-1028.01-92A from Space Telescope Science Institute, which is operated by the Association of universities for Research in Astronomy, Incorporated, under contract NAS5-26555; Sigma Xi, Grants-in-Aid-of-Research; and research funds from Penn State University. DT acknowledges support from MURST.

REFERENCES

- Bershady, M.A., Andersen, D. SubbaRao, M., Connolly, A. 1997, in preparation
- Bershady, M.A., Trevese, D., Kron, R.G. 1991, in *Variability of Active Galactic Nuclei*, eds. H.R. Miller and P.J. Witta (Cambridge University Press), 67
- Burg, R. 1987, Ph.D. thesis, Massachusetts Institute of Technology
- Cheng, F., Danese, L., De Zotti, G., & Franceschini, A. 1985, *MNRAS*, 857
- Connolly, A. J., Csabai, I., Szalay, A. S., Koo, D. C., Kron, R. G. 1995, *AJ*, 110, 2655
- Della Ceca, R., Zamorani, G., Maccacaro, T., Wolter, A., Griffiths, R., Stocke, J.T., & Setti, G. 1994, *ApJ*, 430, 533
- Hartwick, F.D.A., & Schade, D. 1990, *ARAA*, 28, 437
- Hawkins, M.R.S. 1983, *MNRAS*, 202, 571
- Huchra, J. & Burg, R. 1992, *ApJ*, 393, 90

- Kochanski, G.P., Tyson, J.A., Fischer, P. 1996, *AJ*, 111, 1444
- Koo, D.C., Kron, R.G., & Cudworth, K.M. 1986, *PASP*, 98, 285
- Koo, D.C. & Kron, R.G. 1988, *ApJ*, 325, 92 (KK88)
- Kron, R.G. 1980, *ApJS*, 43, 305
- Kron, R.G., Bershad, M.A., Munn, J.A., Smetanka, J.J., Majewski, S.R., and Koo, D.C. 1991, in *The Space Distribution of Quasars*, ed. D. Crampton, ASPCS, 21, 32
- Kron, R.G., & Chiu, L.-T. 1981, *PASP*, 93, 397
- Maccacaro, T., Della Ceca, R., Gioia, I., Morris, S., Stocke, J. & Wolter, A. 1991, *ApJ*, 374, 117
- Majewski, S.R., Munn, J.A., Kron, R.G., Bershad, M.A., Smetanka, and Koo, D.C. 1991, in *The Space Distribution of Quasars*, ed. D. Crampton, ASPCS, 21, 55
- Munn, J. A., Koo, D. C., Kron, R. G., Majewski, S. R., Bershad, M. A., Smetanka, J. J. 1997, *ApJS*, 109, 45
- Pain, R. *et al.* 1996, *ApJ*, 473, 356
- Shanks, T., Georgantopoulos, I., Stewart, G.C., Pounds, K.A., Boyle, B.J., & Griffiths, R.E. 1991, *Nature*, 353, 315
- Tresse, L., Rola, C., Hammer, F., Stasinska, G., Le Fevre, O., Lilly, S. J., Crampton, D. 1996, *MNRAS*, 281, 847
- Trevese, D., Pittella, G., Kron, R.G., Koo, D.C., & Bershad, M. 1989, *AJ*, 98, 108 (T89)
- Trevese, D., Kron, R.G., Majewski, S.R., Bershad, M.A., & Koo, D.C. 1994, *ApJ*, 433, 494 (T94)
- Zitelli, V., Mignoli, M., Zamorani, G., Marano, B., Boyle, B.J. 1992, *MNRAS*, 256, 349

TABLE 1
OPTIMUM APERTURE RADII

m ₄	radii		
	m ₁ -m ₃ <1.05	1.05<m ₁ -m ₃ <1.2	m ₁ -m ₃ >1.2
19.1	12	...	19
20.3	6	7	7
21.2	4	4	4
22.0	3	4	4
22.6	2	4	1
23.1	2	2	1

NOTE.—Radii are in pixel units (0.279 arcsec/pixel), where the central pixel is defined to have radius 0.

TABLE 2
VARIABILITY THRESHOLD DATA

m_4	$m_1 - m_3 < 1.05$		$m_1 - m_3 \geq 1.05$	
	σ_*	σ_{σ_*}	σ_*	$\sigma(\sigma_*)$
20.0	0.021	0.014
20.5	0.029	0.013	0.031	0.013
21.0	0.028	0.011	0.026	0.013
21.5	0.033	0.010	0.034	0.015
22.0	0.043	0.014	0.050	0.018
22.5	0.058	0.018	0.077	0.024
23.0	0.076	0.017	0.101	0.031
23.5	0.100	0.025	0.164	0.041

TABLE 3
CANDIDATE VARIABLE OBJECTS TO $M_4 < 22.5$ OR $J_K < 22$

N_{2540}	Nser	α (1950)	δ (1950)	m_4	J_K	$U - J$	$J - F$	$F - N$	σ^*	σ_N^*	r_1 arcsec	r_{-2} arcsec	m_1 - m_3	z_{spec}	z_{phot}
51	100681	13:05:42.88	29:22:52.4	20.37	19.95	-0.85	0.69	0.71	0.099	5.33	1.04	0.64	1.06	0.403	0.23
1821	114264	13:05:40.52	29:45:07.1	20.77	20.39	-0.35	1.61	0.89	0.079	4.03	1.02	0.62	1.09	0.287	0.51
512	104326	13:06:30.80	29:30:04.3	21.33	20.87	-0.07	0.69	0.56	0.237	14.85	1.04	0.66	1.19	0.215	0.12
1210	110195	13:05:10.46	29:39:02.5	21.43	20.97	-0.37	1.25	0.99	0.143	7.73	1.02	0.63	1.10	0.243	0.39
812	107027	13:04:51.41	29:34:25.2	21.54	21.20	-0.47	1.06	0.89	0.074	2.65	1.02	0.64	1.13	...	0.44
1014	108553	13:04:50.84	29:36:41.1	21.54	20.95	0.15	1.27	1.05	0.213	12.04	1.10	0.70	1.20	0.297	0.30
918	107726	13:06:11.31	29:35:25.3	21.99	21.45	0.08	1.04	0.88	0.208	8.76	0.95	0.58	1.11	...	0.27
1714	113571	13:07:26.70	29:43:57.9	22.01	21.71	-0.22	1.04	0.66	0.098	2.63	1.09	0.71	1.34	0.317?	0.35
769	106596	13:07:20.82	29:33:45.2	22.02	21.36	-0.66	0.61	1.12	0.106	3.01	1.14	0.77	1.20	0.585?	0.39
1249	110459	13:07:11.93	29:39:25.0	22.14	21.37	0.83	1.68	1.11	0.120	3.22	1.20	0.78	1.30	0.324	0.31
2144	116710	13:06:41.13	29:49:03.7	22.30	21.69	-0.34	1.57	0.64	0.136	3.30	1.22	0.81	1.36	?	0.38
635	105334	13:07:21.35	29:31:44.0	22.36	22.24	-0.57	0.99	0.60	0.125	2.54	0.99	0.61	1.09	0.298	0.45
2363	118466	13:05:19.08	29:51:58.5	22.38	21.89	0.70	1.62	1.14	0.148	3.52	1.13	0.73	1.23	...	0.31
2391	118640	13:06:57.41	29:52:20.9	22.49	21.93	0.09	0.79	-0.02	0.205	5.51	1.18	0.77	1.32	0.012?	0.07
204	101951	13:05:30.98	29:25:55.2	22.71	21.72	-0.05	1.58	0.82	0.195	4.07	1.27	0.82	1.23	...	0.39
925	107772	13:07:16.47	29:35:29.3	22.78	21.92	-0.34	0.57	-0.21	0.273	11.12	1.23	0.82	1.00	0.241?	0.06

NOTE.— N_{2540} refers to the serial number from the Rome parent catalogue of 2540 objects used in the analysis, while Nser refers to the matching objects in the catalogue of Koo (1986) as reported by Munn *et al.* (1997). J_K , $U - J$, $J - F$, and $F - N$ are the photographic B_J magnitude and colors from Koo (1986) with the zeropoints adopted by Munn *et al.* (1997). The radii r_1 and r_{-2} are the first and inverse second moments of the light profiles, respectively, from Kron (1980). For reference, faint stars have $r_1 \sim 0.8$ arcsec. Spectroscopic redshifts (z_{spec}) listed with (or as) question marks are based on spectra with less than 2 secure line identifications. In these cases, assigned redshifts are the lowest possible consistent with the identified line(s). Photometric redshifts (z_{phot}) are described in text. *Notes on individual objects:* **Nser 100681** is a spectroscopically confirmed AGN (presence of MgII) with a definite redshift. MgII, [Ne V] $\lambda 3426$, H β , [O III] $\lambda 4959, 5007$ are all probable emission-line detections at moderate S/N from Goldcam and/or Nessie spectra (see text). The spectral continuum is blue, consistent with the broad-band colors. The MgII line in Figure 2a has a FWHM of ~ 30 Å based on a Gaussian fit, as measured with an instrumental spectral resolution of 15 Å. **Nser 114264** is a spectroscopically confirmed AGN (presence of MgII) with a definite redshift based on calcium H, K, MgI (absorption), and [O III] $\lambda 4959, 5007$ (emission) detected at low S/N. **Nser 104326** is a spectroscopically confirmed AGN (variable spectrum) with a definite redshift based on [O II] $\lambda 3727$, [O III] $\lambda 4959, 5007$, and probable H β . **Nser 110195** is a spectroscopically confirmed AGN (broad H α) with definite emission-line redshift based on H γ , H β , [O III] $\lambda 4959, 5007$, H α identified in emission at good S/N. Spectral coverage is not blue enough to detect MgII at this redshift. However, H γ and H α + [N II] appear broad, where the latter has a FWHM=50 Å based on a Gaussian fit, as measured with an instrumental spectral resolution of 15 Å. **Nser 107027** is spectroscopically unobserved. **Nser 108553** has a definite spectroscopic redshift based on a secure identification of [O II] $\lambda 3727$ emission and calcium H absorption, plus probable [O III] $\lambda 5007$ emission. **Nser 107726** is spectroscopically unobserved. **Nser 113571** has one definite detected narrow emission line at 4909 Å which we tentatively assign to [O II] $\lambda 3727$. **Nser 106596** has an uncertain spectroscopic redshift based on possible detection of [O II] $\lambda 3727$ and [Ne III] $\lambda 3869$. [O II] is adjacent to the Na sky-line, and is partially absorbed on the blue side, yet appears substantially stronger than observed residuals from sky subtraction. MgII is in the observed range, but is not identified. **Nser 110459** has a definite spectroscopic redshift based on strong absorption-lines (H, K, G, and MgI bands). The absorption lines, plus a red spectral continuum, consistent with colors, are indicative of a dominant, old stellar population. No line-emission is detected, however spectral coverage does not include MgII or H α . **Nser 116710** has a low S/N spectrum which contains no detected features. A second extended object, 1.4 mag fainter, is separated by 3 arcsec from this candidate. **Nser 105334** has a definite spectroscopic redshift based on strong emission lines of [O II] $\lambda 3727$, [O III] $\lambda 4959, 5007$, and weaker [Ne III] $\lambda 3869$, H γ , and H β . While the spectrum is not flux calibrated, the apparent weakness of H β with respect to [O II] and [O III] is indicative of Seyfert 2 spectrum. A second extended object, 1.6 mag fainter is separated by 3.5 arcsec from this candidate. **Nser 118466** is spectroscopically unobserved. A second extended object, 1.6 mag fainter is separated by 3.5 arcsec from this candidate. **Nser 118640** has an uncertain spectroscopic redshift based on one probable emission line tentatively identified as H α . An 0.1 mag brighter stellar object is separated by 5 arcsec from Nser 118640. **Nser 101951** is spectroscopically unobserved. **Nser 107772** has an uncertain spectroscopic redshift based on one probable emission line tentatively identified as [O III] $\lambda 5007$.

Fig. 1.— Weighted root-mean-square deviation of the magnitude differences with respect to the mean for each object, over the 11 year baseline, as a function of J magnitude on MPF 1053 ($m_4(1053)$) for the 1636 objects in the survey. The variability criteria for compact ($m_1-m_3 < 1.05$) and diffuse sources ($m_1-m_3 > 1.05$) are indicated by the dashed and solid lines respectively. These are derived from the photometric errors (Table 2). For $m_4 < 22.4$, a 2.5σ threshold is imposed (lower dashed and solid curves); for $m_4 > 22.5$, a 3.5σ threshold is imposed (upper dashed and solid curves). Variable candidates are specially marked in categories of: spectroscopically confirmed AGN, close to neighboring objects, or otherwise as a function of image compactness. Four unmarked objects above thresholds for $m_4 < 22.5$ are multiply matched between two independent catalogues, as discussed in text. Arrows point to two candidates with $m_4 > 22.5$ but $J_K < 22$.

Fig. 2.— (a) Spectra of four variable candidates from the KPNO 4m telescope (instrumental configurations and exposures differ for each object, as described in Munn *et al.* 1997). Three spectra confirm the presence of AGN (Nser 100681, 114264, and 110195), as discussed in the text. A fourth spectrum (Nser 110459) yields a reliable redshift. Confirmed lines are detailed in the Notes to Table 3, while positions of common emission/absorption lines are marked here at the appropriate redshift for reference.

Fig. 2.— (b) Spectra of six variable candidates from the WIYN 3.5m telescope and Hydra multi-fiber spectrograph (3 arcsec fibers, 400 lines/mm grating, spectral resolution $[\lambda/\Delta\lambda]$ of ~ 780 , three hours integration for Nser 113571, 106596, 105334, six hours integration for Nser 107772, nine hours integration for Nser 108553, 118640). Two objects (Nser 108553 and 105334) have secure redshifts based on strong multiple emission or absorption lines. For Nser 105334, note the weakness of $H\beta$ relative to $[O III] \lambda 4959, 5007$ and $[O II] \lambda 3727 \text{ \AA}$, which identifies this source as a possible Seyfert 2. In all other cases there is insufficient evidence for the presence of an AGN. Confirmed lines are detailed in the Notes to Table 3, while positions of common emission/absorption lines are marked here at the appropriate redshift for reference.

Fig. 2.— (c) Spectra of Nser 104326 taken ~ 6 years apart but with the same aperture. (See caption to Figure 2a and 2b for descriptions of observations.) The spectra show dramatically different continuum shapes and emission-line equivalent widths.

Fig. 3.— Light-curves for the 16 candidate variables in Table 3, ordered by m_4 . Magnitudes (m), and their uncertainties (1 sigma) are defined within the optimum aperture (Table 1) and are plotted with respect to the average magnitude ($\langle m \rangle$).

Fig. 4.— Image compactness (m_1-m_3) as a function of J magnitude [$m_4(1053)$] for the same sample in Figure 1. Variable candidates are specially marked in categories of:

spectroscopically confirmed AGN, close to neighboring objects, or otherwise as a function of $U - J$ color. The dashed line at $m_1 - m_3 = 1.05$ demarks regions where objects are nominally stellar or extended. Arrows point to two candidates with $m_4 > 22.5$ but $J_K < 22$.

Fig. 5.— $U - J$ color as a function of J magnitude [$m_4(1053)$] for the same sample in Figure 1. Variable candidates are specially marked in categories of: spectroscopically confirmed AGN, close to neighboring objects, or otherwise as a function of image compactness. Arrows point to two candidates with $m_4 > 22.5$ but $J_K < 22$.

Fig. 6.— (a) $U - J$ color as a function of image compactness ($m_1 - m_3$) for survey objects in the range $20 < m_4 < 22.5$. Variable candidates are specially marked in categories of: spectroscopically confirmed AGN, close to neighboring objects, or otherwise as a function of normalized σ^* (σ^*_N). The dashed line at $m_1 - m_3 = 1.05$ demarks regions where objects are nominally stellar or extended.

Fig. 6.— (b) $U - J$ color as a function of image compactness ($m_1 - m_3$) for survey objects in the range $m_4 > 22.5$. Variable candidates are specially marked according to the normalized σ^* (σ^*_N). The dashed line at $m_1 - m_3 = 1.05$ demarks regions where objects are nominally stellar or extended. Arrows point to two candidates with $m_4 > 22.5$ but $J_K < 22$.

Fig. 7.— Apparent magnitude (J_K) vs. redshift for objects in SA 57: spectroscopically confirmed QSOs (T94), extended galaxies with secure spectroscopic redshifts (dots, Munn *et al.* 1997), and the 16 variable candidates from Table 3, here (see key). In cases where spectroscopic redshifts (z_{spec}) are not available for the variable candidates, photometric redshifts (z_{phot}) are used instead. Lines of constant luminosity for $M_B = -23$ and -21 are drawn assuming $H_0 = 50 \text{ km s}^{-1} \text{ Mpc}^{-1}$, $q_0 = 0.5$ and $\alpha = -1$.

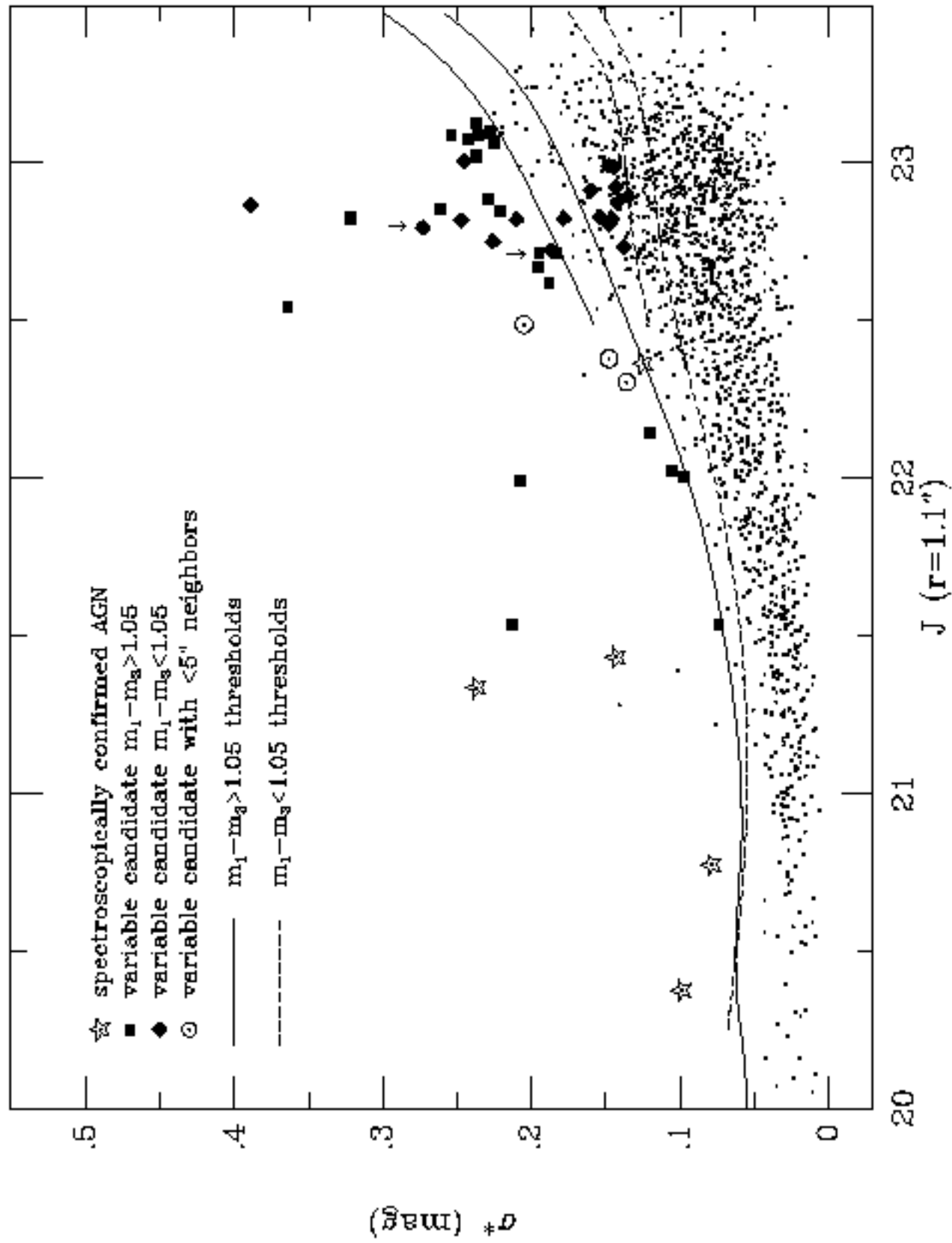


Fig. 1

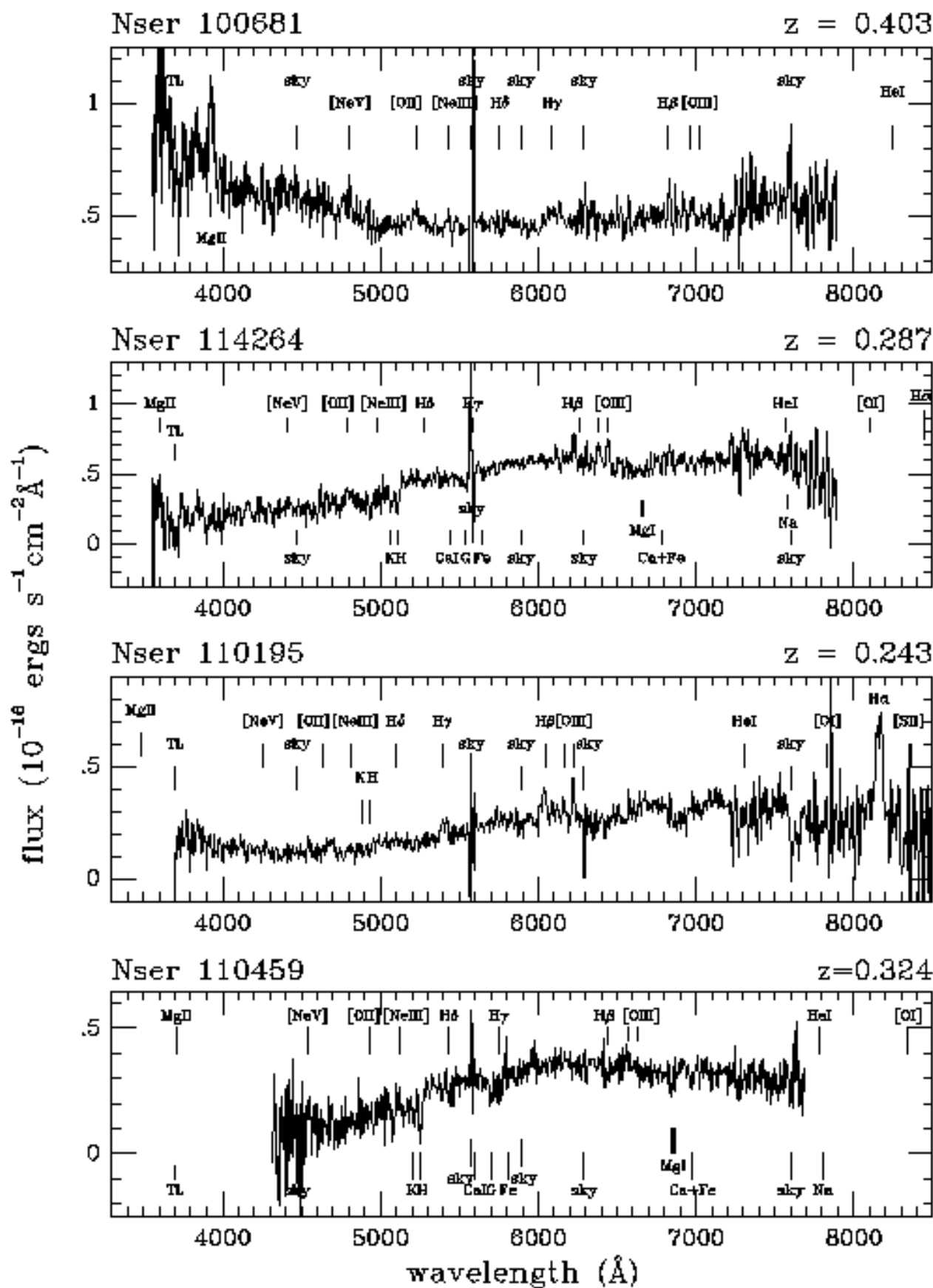


Fig. 2a

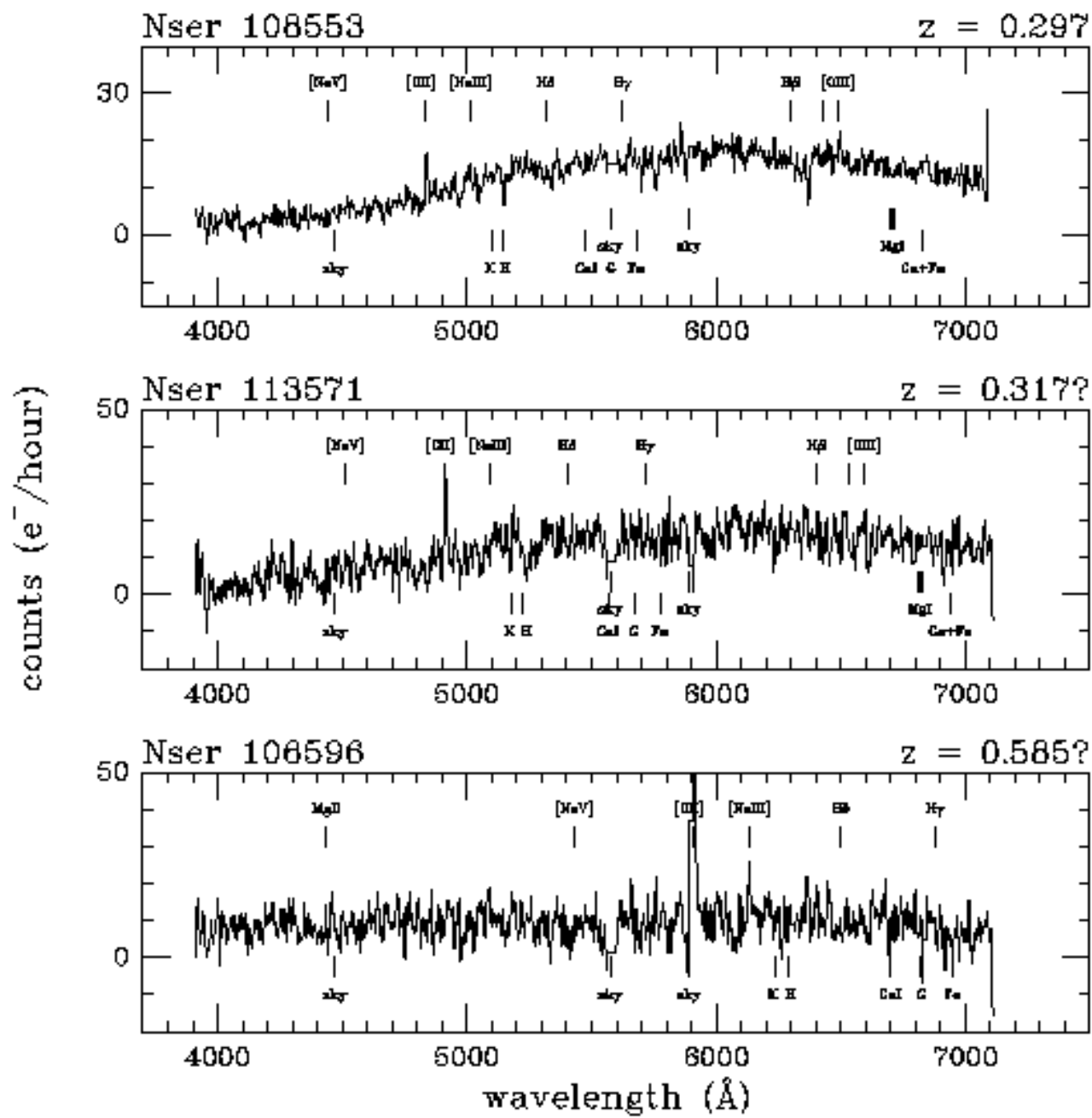


Fig. 2b

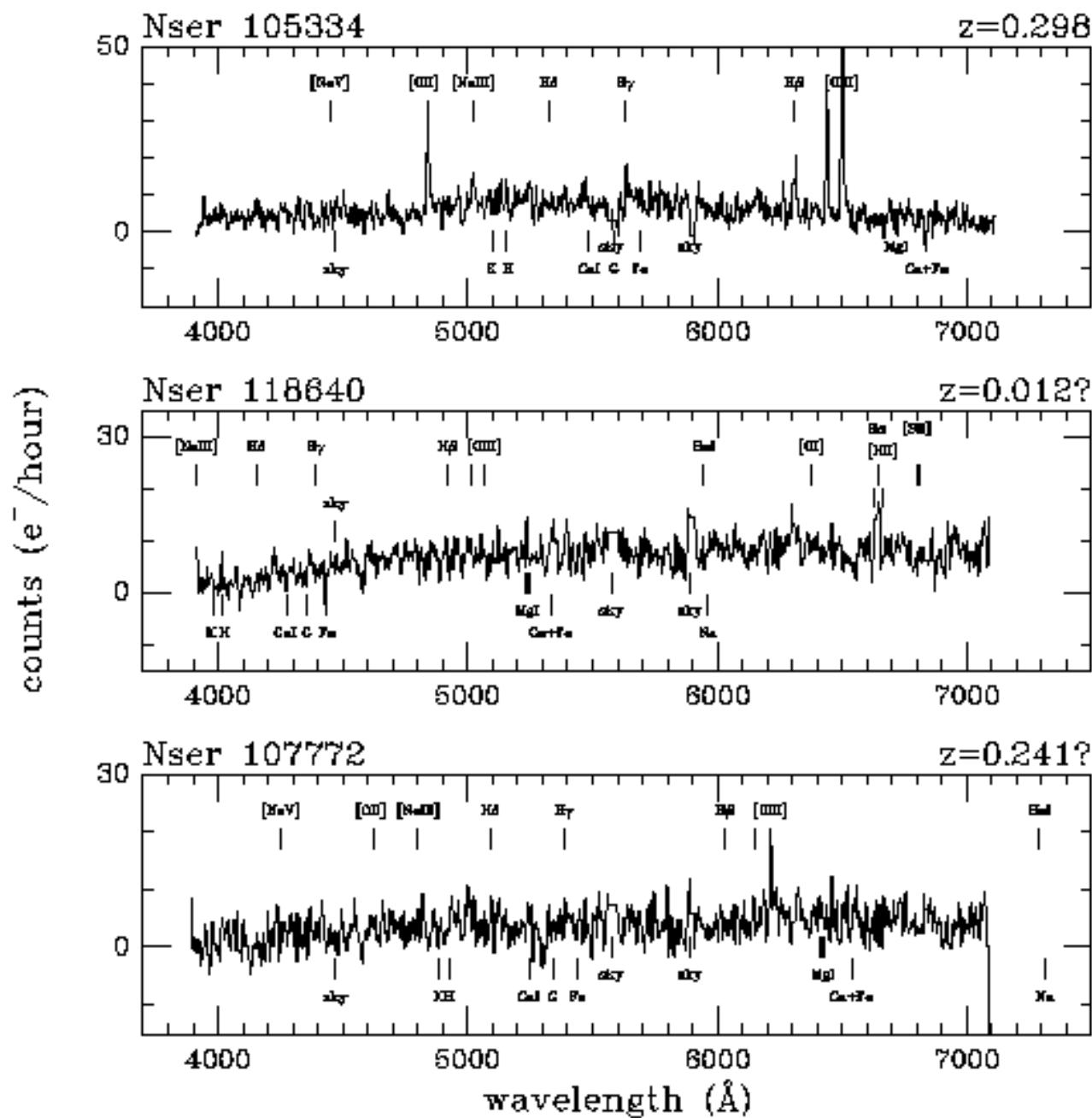


Fig. 2b (continued)

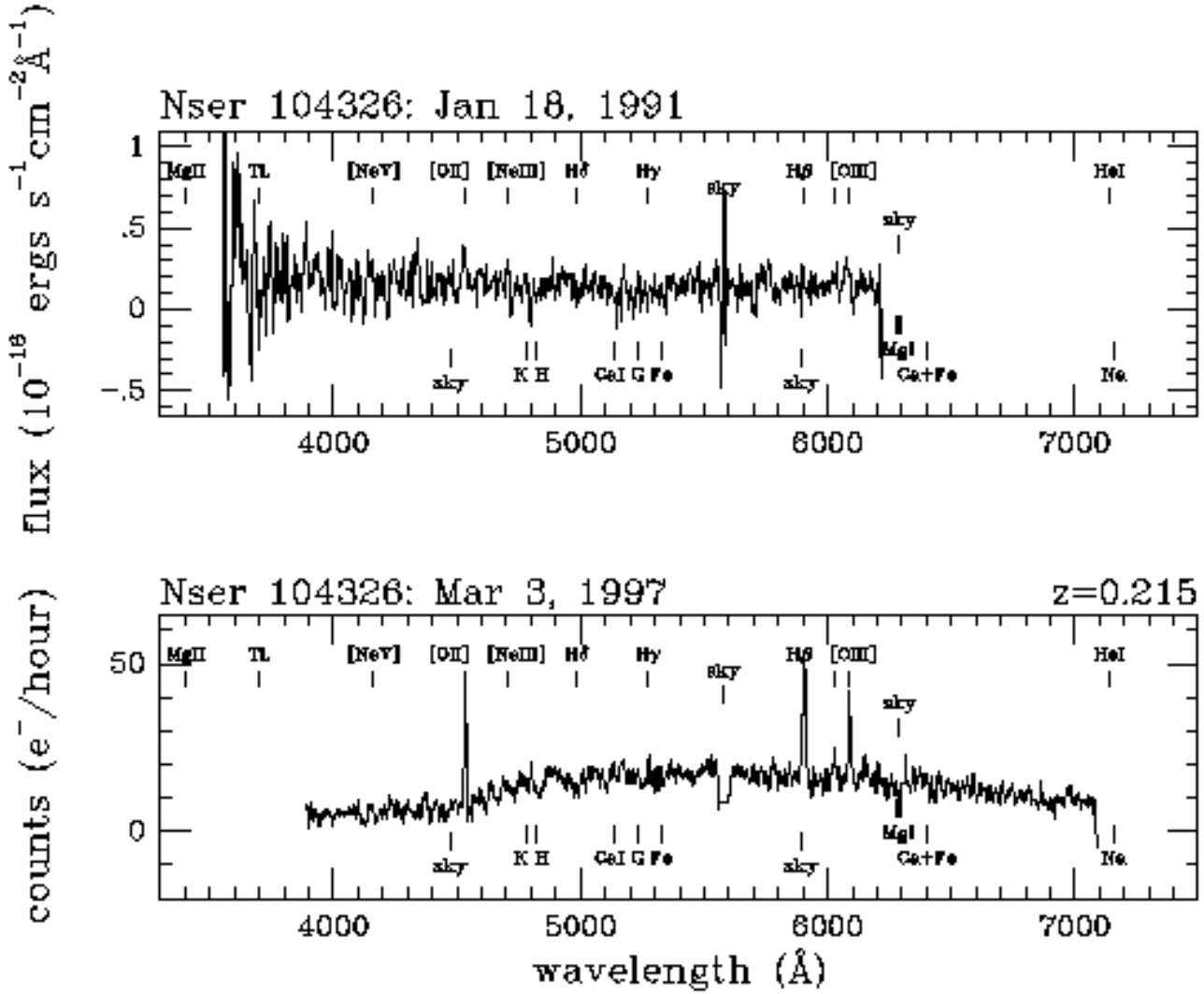


Fig. 2c

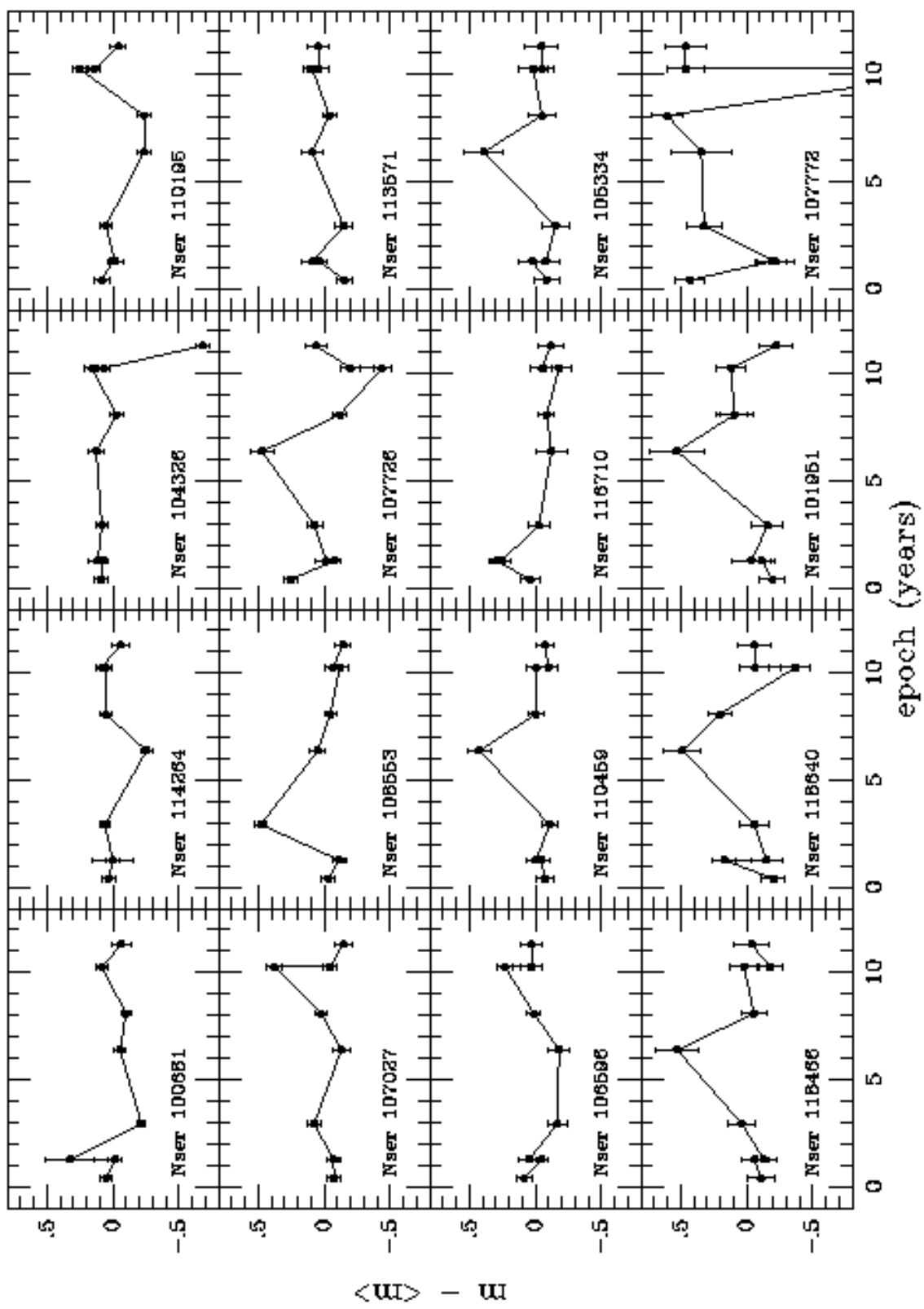


Fig. 3

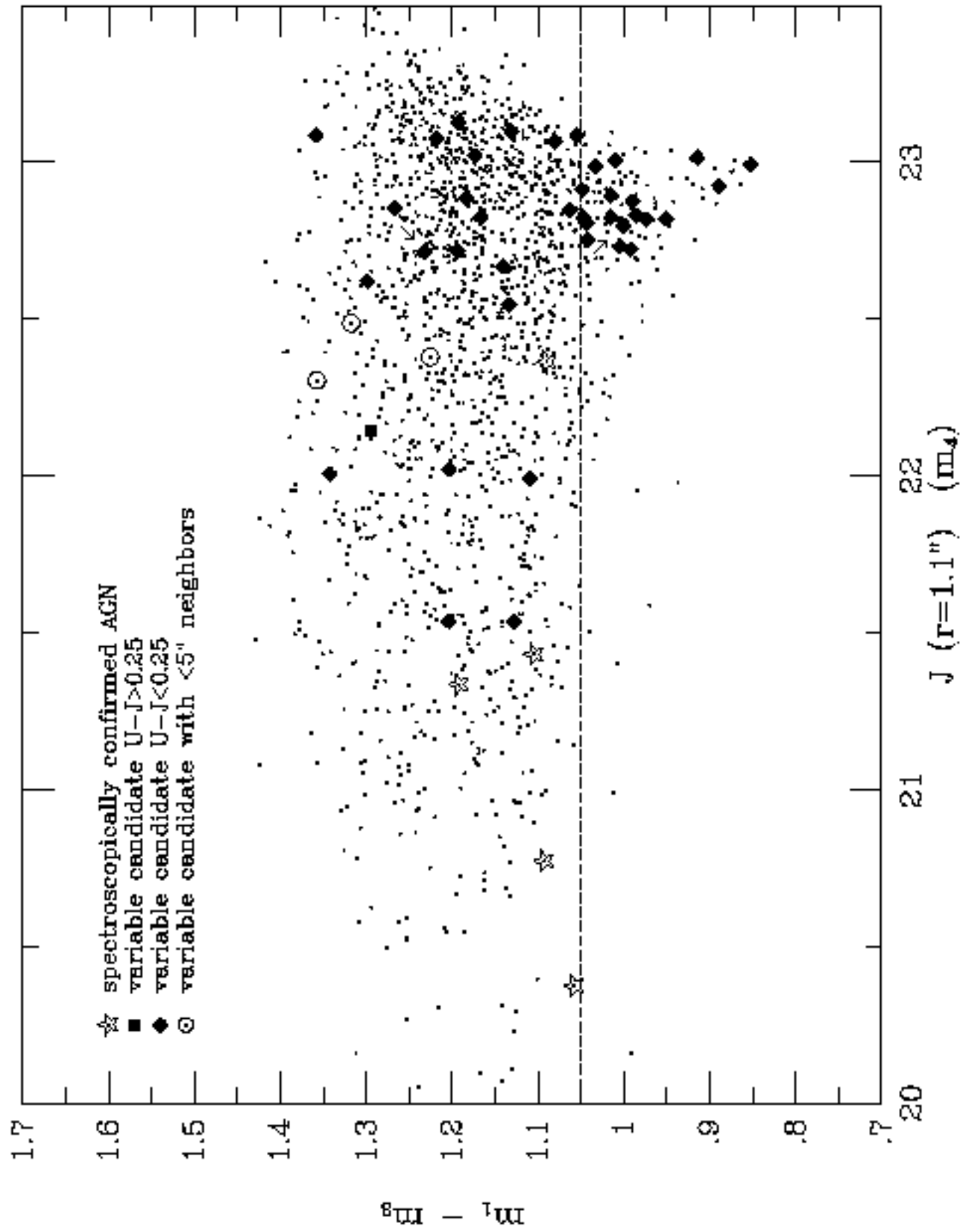


Fig. 4

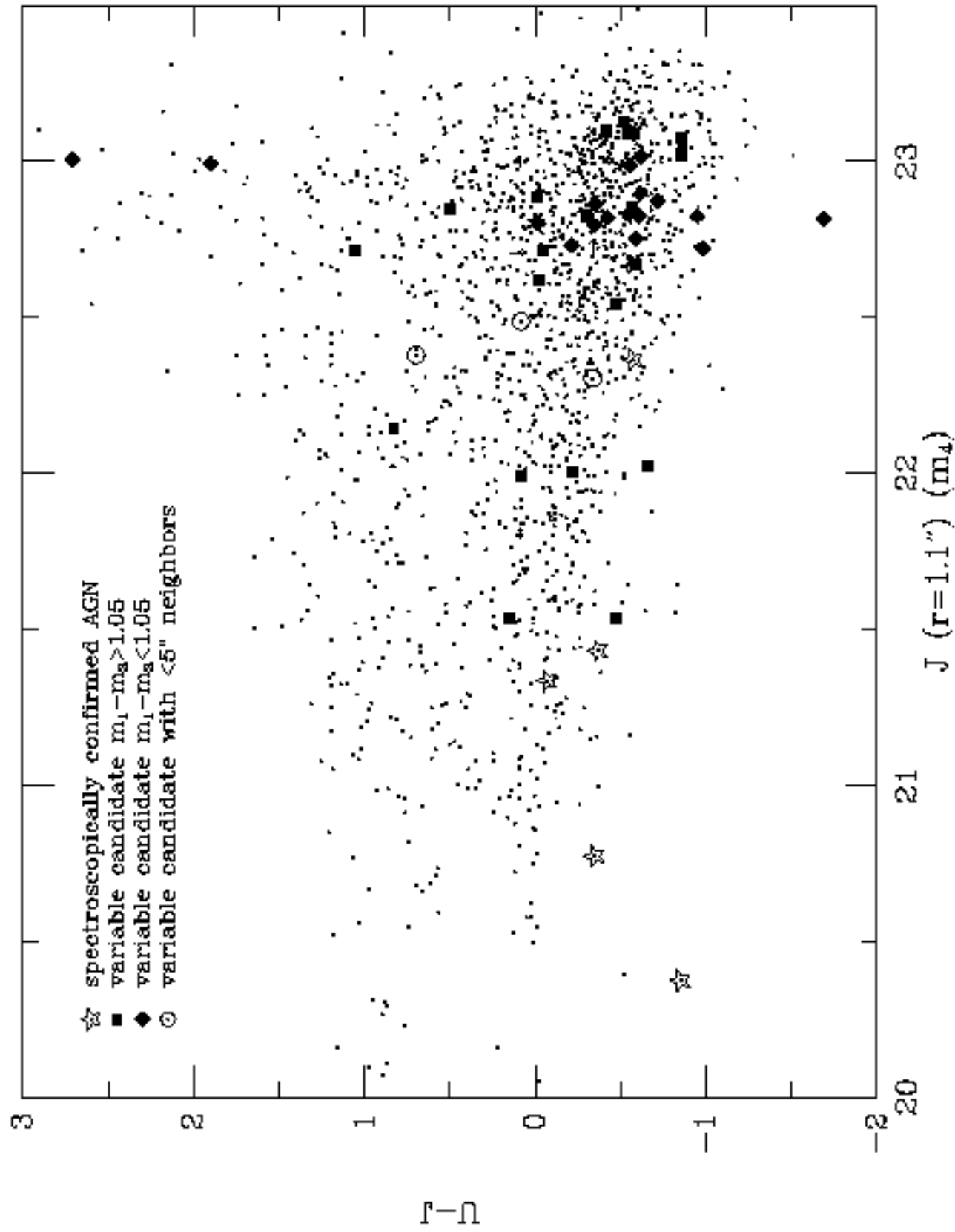


Fig. 5

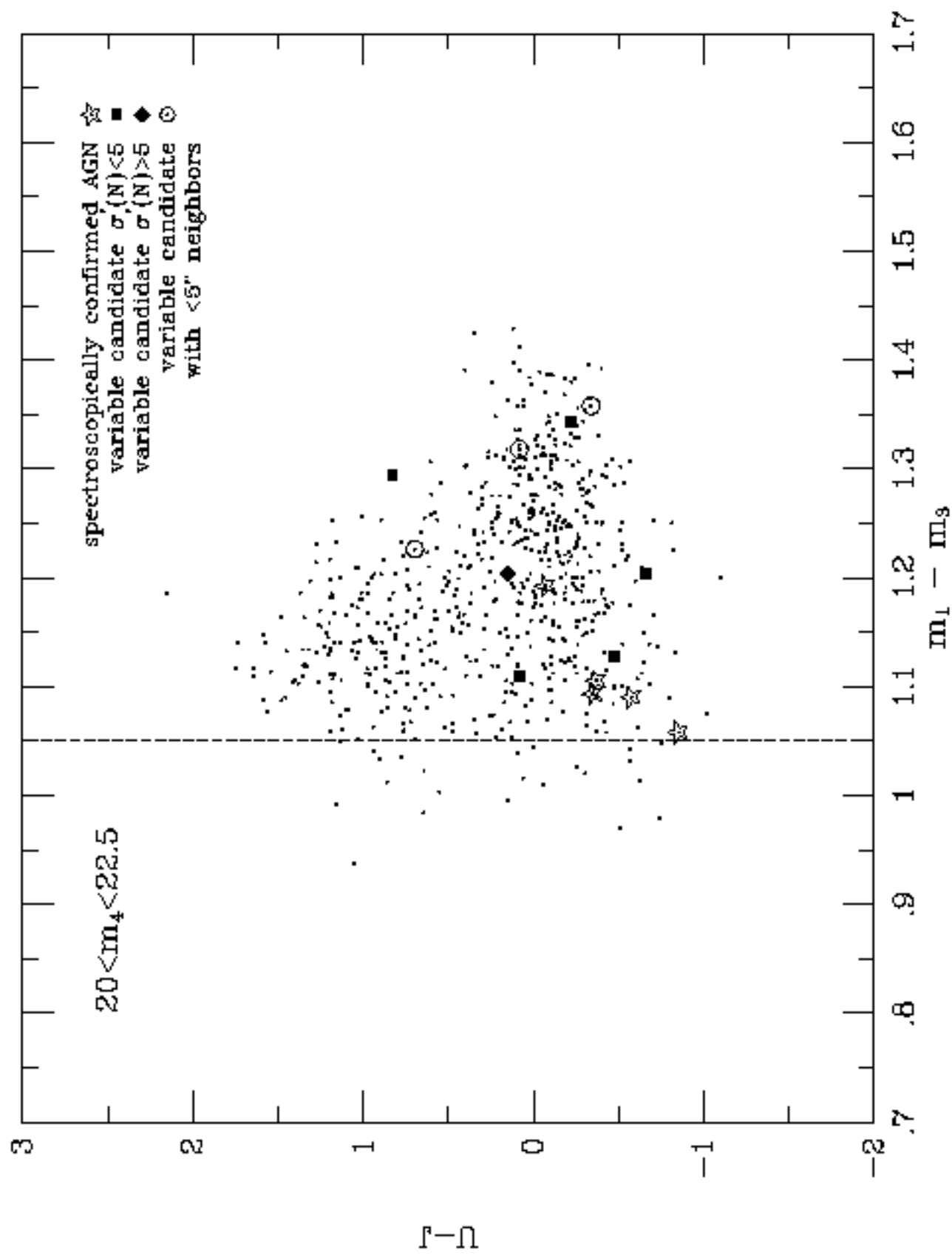


Fig. 6a

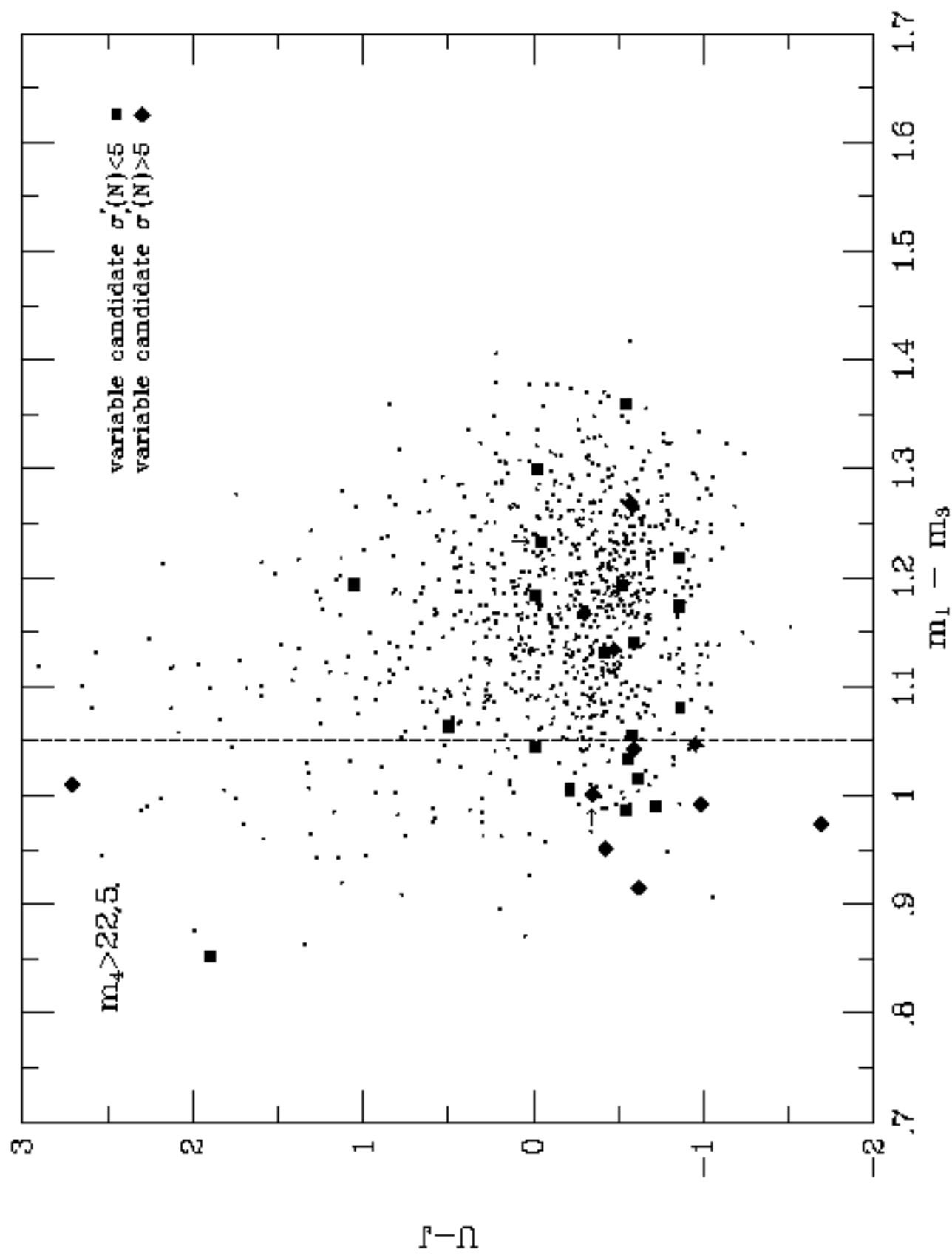


Fig. 6b

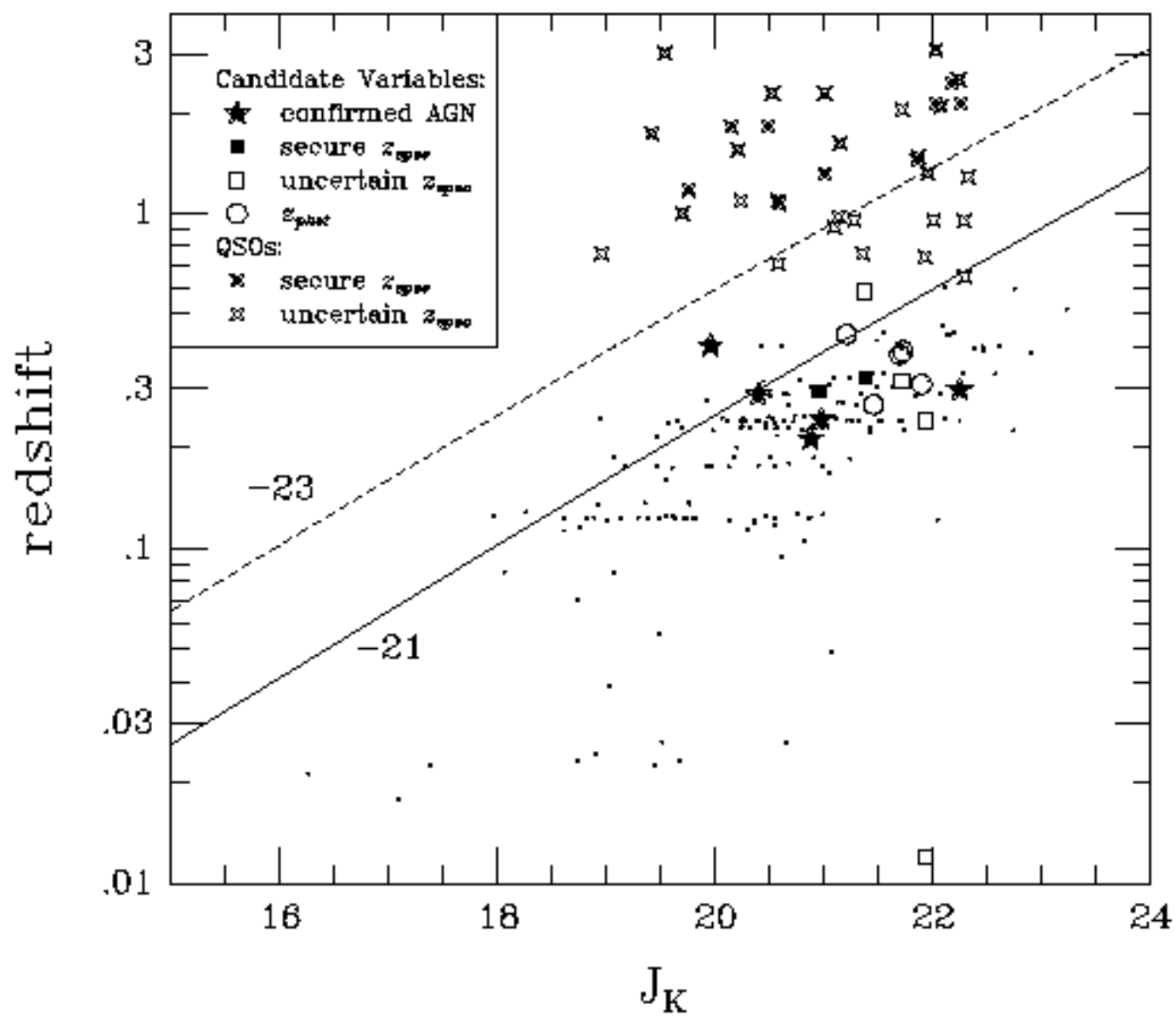


Fig. 7